

1 Avalanche Statistics of Driven Granular Slides in a
2 Miniature Mound

D.E. Juanico, A. Longjas, R. Batac, and C. Monterola

3 National Institute of Physics, University of the Philippines , Quezon City,
4 Philippines

arXiv:0805.1582v2 [nlin.AO] 24 Aug 2008

cmonterola@nip.upd.edu.ph,cmonterola@gmail.com

5 We examine avalanche statistics of rain- and vibration-driven granular slides
6 in miniature sand mounds. A crossover from power-law to non power-law avalanche-
7 size statistics is demonstrated as a generic driving rate ν is increased. For
8 slowly-driven mounds, the tail of the avalanche-size distribution is a power-
9 law with exponent -1.97 ± 0.31 , reasonably close to the value previously
10 reported for landslide volumes. The interevent occurrence times are also an-
11 alyzed for slowly-driven mounds; its distribution exhibits a power-law with
12 exponent -2.670 ± 0.001 .

13 *Introduction.*—Landslides are the movement of a mass of rock, debris, or earth down a
14 slope triggered by a variety of natural factors, ranging from rainfall to volcanic activity.
15 On 17 February 2006, a series of mudslides caused widespread damage and loss of life in
16 Southern Leyte, Philippines. The deadly landslides followed a ten-day period of persistent
17 downpour and a minor ($M2.6$) earthquake [Catane *et al.*, 2007].

18 One practical approach in analyzing the underlying physical processes that generate
19 landslide statistics is numerical modeling. One class of models, based on *self-organized*
20 *criticality* (SOC) [Hergarten and Neugebauer, 1998; Piegari *et al.*, 2006], hint at some
21 possible mechanisms yielding the observed statistics. SOC is a theory underlying the
22 spontaneous emergence of critical-like behavior (i.e., power laws and critical exponents)
23 in systems for which the timescales between buildup and release of stress are separated,
24 and for which the stress-transfer mechanism is generally nonconservative [Juanico *et al.*,
25 2007a, b; Juanico and Monterola, 2007]. SOC concepts have aroused great interest in
26 the study of granular matter [Jaeger *et al.*, 1989], a well-known example of which is the
27 ricepile experiment [Frette *et al.*, 1996].

28 The present work examines avalanche statistics of rain- and vibration-driven granular
29 slides in miniature sand mounds. A previous study [Katz and Aharonov, 2006] explored
30 slope-failure types due to horizontal and vertical vibrations in a miniature sandbox. It
31 was shown that vertical shaking leads to a power-law distribution of slide-block surface
32 area, although the experiment did not demonstrate a ‘rollover’ observed in substantially
33 complete, empirical landslide inventories [Guzzetti *et al.*, 2002; Malamud *et al.*, 2004a, b].
34 In the present study, we incorporate rainfall as a triggering mechanism and show that

its presence allows our model to capture the rollover. Likewise, we demonstrate experimentally the existence of a crossover from power-law to non power-law statistics as theoretically predicted by *Piegari et al.* [2006].

It appears from the data reported by *Malamud et al.* [2004a] that any type of trigger (earthquake, rainfall, or snowmelt) yields roughly the same trend in the landslide-size distribution. Combining any two trigger types should reasonably yield the same trend in the distribution, and this is precisely one of the aspects tested in this study. In addition, the computational model proposed here assumes a generic triggering mechanism. Thus, rainfall and vibrations have been introduced to act as concurrent landslide triggers.

Experimental Method.—The experimental setup (Figure 1) consists of a sand mound (total mass, 1500 g) disturbed concurrently by rainfall and vibration. River sand with irregularly-shaped grains (mean grain mass, 8.8×10^{-4} g; mean grain volume, 5.8×10^{-4} cm³) was used. Initially, the mound is dry and is a near-perfect cone in shape with a base diameter of 23 cm and height of 8 cm (slope angle $\approx 35^\circ$ with respect to horizontal). Water (200 ml) is dispensed quite uniformly over the surface and allowed time to seep into the mound. The wet mound thus consists of 12% water by weight at the start of the observations.

Rainfall is simulated using a makeshift sprinkler (water capacity, 75 ml) placed directly above the mound apex. Water pours out through a circular orifice of diameters: 4.5, 10.0, and 47.0 (± 0.5) mm. Pour rate is the mass of water flowing out per unit time, and the orifice diameter controls its value. Pour rate is constant at the following values: 3.21 g s^{-1} ; 6.60 g s^{-1} ; and 21.09 g s^{-1} over a time interval of 20, 10, and 3 s, respectively. These

57 time intervals are commensurate with the length of time the 75-ml water in the sprinkler
58 is depleted.

59 Horizontal vibrations are applied using a tabletop earthquake simulator. Horizontal
60 shaking at low to moderate accelerations generates grain flows of the topmost layer of the
61 slope resulting in rapid failure-plane development [*Katz and Aharonov, 2006*]. As shown
62 in Figure 1, a translational-load platform, powered by a servo motor driven by a USB 6009
63 DAQ driver (National InstrumentsTM), imparts the horizontal vibrations having a saw-
64 tooth wave profile. The wave profile is fed into the DAQ driver via LabVIEWTM computer
65 interface. The wave is characterized by a maximum amplitude of 1.5 cm (with respect
66 to center) and by frequencies of: 1.8 Hz, 10 Hz, and 89 Hz. Due to the 3D shape of the
67 mound, slope-parallel and slope-normal accelerations are both present during shaking.

68 *Computational Model.*—The underlying physics of the avalanche statistics of driven
69 granular slides is investigated by performing numerical experiments of a landslide model
70 proposed by *Piegari et al. [2006]*, defined as follows. A mountain ‘slope’ is represented as
71 a 2D inclined plane partitioned into a grid (500 cells \times 500 cells). Each cell k is described
72 by a stress parameter θ_k initialized randomly between 0 and 1 from an arbitrarily chosen
73 rectangular distribution (although the distribution used for initial randomization does
74 not affect the long-term behavior of the model [*Piegari et al., 2006*]). The randomization
75 captures the expected heterogeneity of stress values in actual mountain slopes. Stress in
76 the slope builds up over time by means of a localized (i.e., cell scale) driving: $\theta_k(t + \Delta t) =$
77 $\theta_k(t) + \nu\Delta t$, where ν is the generic driving rate. For simplicity, it is assumed that ν has
78 the same value for all cells. When a cell k has $\theta_k > 1$, it relaxes by transferring stress to

79 its four nearest neighbors $nn = \{up, down, right, left\}$ at different proportions g_{nn} . By
 80 virtue of gravity, stress transfer is biased downwards, such that: $g_{down} > g_{up}$, subject to
 81 the constraint $g_{down} + g_{up} = 0.5$; and $g_{left} = g_{right} = 0.25$. In this study, it is assumed that
 82 transfer is conservative, so that $\sum_{nn} g_{nn} = 1$. Stress-transfer proceeds until the entire
 83 grid relaxes so that for all k , $\theta_k < 1$. All consecutive stress-transfers comprise a landslide
 84 at time t , and the total number of collapsing cells at time t is the landslide area $A(t)$.
 85 For correspondence with experiments, although we recognize its limitations, we assume a
 86 landslide mass-area relation: $M \sim A^{3/2}$, which can be derived by means of dimensional
 87 analysis (i.e., assuming that M is proportional to volume V , and then considering that
 88 $V \sim A^{3/2}$ [Hovius *et al.*, 1997]).

89 The novelty of our computational modeling approach is in considering the gradual
 90 flattening of the slope after several landslides have occurred (as seen in our experiments).
 91 An update rule is introduced to decrease g_{down} , as follows: $g_{down}(t + \Delta t) = g_{down}(t) -$
 92 $10^{-5}A(t)$, where $A(t)$ is the area of landslide at time t . The value of g_{up} is updated
 93 accordingly via the constraint $g_{down} + g_{up} = 0.5$. This modification incorporates the
 94 dynamics of slope evolution which was not realized by Piegari *et al.* [2006]. The generic
 95 driving rate ν defined in the model corresponds to the experimental parameters, as shown
 96 in Table 1.

97 *Results and Discussion.*—Avalanche size is interpreted as the total mass M of wet sand
 98 falling from the mound onto the basin within a 20-ms period (temporal resolution of our
 99 data-capturing device). M is measured by a weighing scale (resolution, 0.1 g) beneath
 100 the basin, as illustrated in Figure 1. M is sometimes contributed to by several distinct

101 ‘sub-avalanches.’ The tradeoff in this interpretation is that although it resolves mostly
 102 individual avalanches, those that last > 20 ms may be recorded as partial sub-avalanches,
 103 and if there are more than one avalanche within any 20 -ms interval, these will be recorded
 104 as one value.

105 The total observation period is determined by the pour rate and is based on how long
 106 before the entire mound washes out. A total of 20, 10, and 3 trials were made for slow,
 107 moderate, and fast pour rates, respectively. The fact that sand tends to stick together
 108 when wet (i.e., negative pore pressure) [Katz and Aharonov, 2006] justifies our assumption
 109 that by measuring the mass M of falling wet sand, the avalanche volume is effectively mea-
 110 sured (i.e., $M \propto V$). In [Malamud *et al.*, 2004a, b], the distribution of landslide volumes
 111 has been deduced from scaling arguments due to the difficulty in obtaining direct informa-
 112 tion about landslide volume from field data [Malamud *et al.*, 2004a]. In our experiment,
 113 landslide volume distribution is determined by using mass as a proxy for volume.

114 Figure 2 illustrates probability densities (pdf) of avalanche sizes resulting from slow (\blacklozenge),
 115 moderate (\bullet), and fast (\blacksquare) driving (as defined in Table 1). Also shown are corresponding
 116 pdfs from numerical simulations of the computational model. The pdfs for all cases exhibit
 117 peaks that shift towards the right as the driving rate is increased. In particular, The tail of
 118 the pdf for a slowly-driven mound (\blacklozenge , Fig. 2) is a power-law with exponent $-1.97(\pm 0.31$;
 119 standard error of least-squares fit, $df = 4$, reduced $\chi^2 = 1.14 \times 10^{-5}$), determined by
 120 curve-fitting the linear portion (in double log scale) for which $1.0 \text{ g} < M < 8.0 \text{ g}$. The
 121 exponent value is not significantly different (two-tailed t -test: $t = 1.13$, $df = 4$, $p = 0.32$)

122 from the value -1.93 reported for probability densities of landslide volumes [*Malamud*
123 *et al.*, 2004a].

124 A crossover from power-law to non power-law statistics is also evident in our data. This
125 crossover has been previously recognized by *Piegari et al.* [2006] as an effect of increasing
126 the generic driving rate ν . We attribute the crossover to timescale separation. Based
127 on the model, the timescale separation is the ratio between the timescale ν^{-1} of stress
128 changes on any site due to driving and the timescale of the longest avalanche which is set
129 at $\Delta t = 1$. Hence, the timescale separation is $(\nu\Delta t)^{-1} \sim \nu^{-1}$. For slow driving (small ν),
130 SOC theory expects the appearance of power laws. On the other hand, for fast driving,
131 a different trend is expected. We found this fit to resemble a normal distribution, and is
132 centered at a large M (■, Fig. 2). An implication of the crossover is that under high-rate
133 driving (especially by frequent rainfall), the landslide behavior of mountain slopes appears
134 to produce relatively large avalanches on average. It is thus not surprising that highly-
135 devastating rain-induced landslides occur more often in areas frequently struck by storms.
136 However, a more comprehensive description of ν should incorporate ground-failure factors
137 such as soil composition. Such factors have been neglected in this study for simplicity.

138 The rollover observed in our data supports the claim that the rollover seen in sub-
139 stantially complete landslide-inventory datasets is not a mere artifact of limited mapping
140 resolution [*Guzzetti et al.*, 2002; *Malamud et al.*, 2004a, b]. As $\nu \rightarrow 0$, the rollover is
141 expected to disappear thus leaving the power-law tail of the distribution. This agrees
142 with predictions from the Olami-Feder-Christensen model [*Olami et al.*, 1992], which is
143 the limiting case of our model for $\nu \rightarrow 0$. To the extent that our experiment and numerical

144 results agree, we thus attribute the rollover to the finiteness, albeit small, value of the
 145 driving rate ν assumed to characterize real physical systems. From this argument it can
 146 thus be reasonably deduced that the rollover increases in prominence, such that the peak
 147 shifts towards larger avalanche sizes, as ν increases. We found that at $\nu \sim 7.5 \times 10^{-4}$,
 148 the avalanche size distribution more closely resembles a normal (or Gaussian) distribution
 149 that is centered at a large size value.

150 A relevant aspect for hazard prediction is the interevent occurrence time (IOT) statis-
 151 tics. The IOT is the interval between the peaks of events whose sizes are above a given
 152 threshold ($M = 0.5$ g), which corresponds roughly to the peak of the pdf (\blacklozenge , Figure 2).
 153 We thus gathered time series of avalanche size $M(t)$ in slowly-driven mounds over a period
 154 of 20 s. Figure 3 illustrates a representative sample for the first 10 s of this time series for
 155 both experiment and computational data. A thresholding procedure is applied to discard
 156 events whose sizes are below the threshold. The region $M < 0.5$ g corresponds to the
 157 rollover portion of the pdf (\blacklozenge , Figure 2) for slowly-driven mounds. The vertical demar-
 158 cation line in Figure 2 corresponds to the horizontal demarcation line in Figure 3. The
 159 probability density for interevent occurrence time derived from experiment and model are
 160 shown on the inset graph of Figure 3 (\blacktriangle ; blue, solid curve), and both exhibit a power-law
 161 trend with exponent $-2.670(\pm 0.001)$; standard error of least-squares fit, $df = 6$, reduced
 162 $\chi^2 = 2.09 \times 10^{-8}$.

163 A power-law IOT distribution implies that most correlated events (i.e., those with sizes
 164 above the threshold) tend to occur close together in time, which seems to agree with
 165 recent findings [Rossi *et al.*, 2008]. The power-law trend further implies that correlated

166 events may be separated a long time from each other—a landslide today may be linked
167 with an earlier landslide a long time ago. This may be tied to the fact that landslides tend
168 to occur where they have occurred before. The long temporal correlation suggested by
169 the power-law could possibly be attributed to rainfall seasonal trends [*Rossi et al.*, 2008].

170 To illustrate that a power-law emerges from temporal correlations in the time series
171 data, a shuffling procedure has been implemented wherein the order of the time series
172 is rearranged randomly [*Yang et al.*, 2004]. Random shuffling effectively eliminates any
173 trace of correlations present in the original time series data. The thresholding procedure
174 is then applied on the shuffled data to extract the IOT distribution. After shuffling, the
175 IOT distribution becomes exponential, as shown in Figure 3 (▼, Inset). The change from
176 power-law to exponential due to shuffling has been expected for systems governed by SOC
177 dynamics [*Woodward et al.*, 2004]. Therefore, we conclude that the power-law is a direct
178 indication of temporal correlations in the time series data.

179 *Conclusion.*—The general agreement of our results with empirical data suggests that
180 miniature experimental models may help in understanding several underlying facets of
181 complex landslide processes. While several geophysical factors such as sand porosity,
182 rock type, pore-water pressure, and humidity have been neglected, the landslide model
183 presented here delivers basic insights that would guide more detailed explorations later
184 on.

185 **Acknowledgments.**

186 The authors gratefully acknowledge B.D. Malamud for his insightful comments on our
187 manuscript. We also thank B. Buenaobra for assistance on instrumentation; O. Burgos

188 and M. Abundo for the earthquake simulator; and funding from the UP-OVPAA (C.M.),
 189 UP-OVCRD (D.E.J. and C.M.), and DOST (A.L. and R.B.).

References

- 190 Catane, S., H.B. Cabria, C.P. Tomarong, R.M. Saturay, M.A.H. Zarco and W.C. Pio-
 191 quinto (2007), Catastrophic rockslide-debris avalanche at St. Bernard, Southern Leyte,
 192 *Landslides*, *4*, 85.
- 193 Frette, V., K. Christensen, A.M. Malthé-Sørensen, J. Feder, T. Jøssang and P. Meakin
 194 (1996), Avalanche dynamics in a pile of rice, *Nature*, *379*, 49.
- 195 Guzzetti, F., B. Malamud, D. Turcotte, and P. Reichenbach (2002), Power-law correlations
 196 of landslide areas in central Italy, *Earth Planet. Sci. Lett.*, *195*, 169.
- 197 Hergarten, S. and H. Neugebauer (1998), Self-organized criticality in a landslide model,
 198 *Geophys. Res. Lett.* , *25*, 2382.
- 199 Hovius, N., C.P. Stark, and P.A. Allen (1997), Sediment flux from a mountain belt derived
 200 by landslide mapping, *Geology*, *25*, 231.
- 201 Jaeger, H.M., C.H. Liu, and S.R. Nagel (1989), Relaxation at the angle of repose, *Phys.*
 202 *Rev. Lett.*, *62*, 40.
- 203 Juanico, D.E., C. Monterola, and C. Saloma (2007a), Self-organized critical branching in
 204 systems that violate conservation laws, *New J. Phys*, *9*, 92.
- 205 Juanico, D.E., C. Monterola, and C. Saloma (2007b), Dissipative self-organized branching
 206 in a dynamic population, *Phys Rev. E*, *75*, 045105R.
- 207 Juanico, D.E. and C. Monterola (2007), Background activity drives criticality of neuronal
 208 avalanches, *J. Phys. A*, *40*, 9297.

- 209 Katz, O. and E. Aharonov (2006), Landslides in a vibrating sand box: What controls
210 types of slope failure and frequency magnitude relations?, *Earth Planet. Sci.*, *247*, 280.
- 211 Malamud, B., D. Turcotte, F. Guzzetti and P. Reichenbach (2004a), Landslide inventories
212 and their statistical properties, *Earth Surf. Process. Land.*, *29*, 687.
- 213 Malamud, B., D. Turcotte, F. Guzzetti and P. Reichenbach (2004b), Landslide, earth-
214 quakes, and erosion, *Earth Planet. Sci. Lett.*, *229*, 45.
- 215 Olami, Z., H.J.S. Feder and K. Christensen (1992), Self-organized criticality in a contin-
216 uous nonconservative cellular automaton modeling earthquakes, *Phys. Rev. Lett.*, *68*,
217 1244.
- 218 Piegari, E., V. Cataudella, R. Di Maio, L. Milano and M. Nicodemi (2006), A cellular
219 automaton for the factor of safety field in landslides modeling, *Geophys. Res. Lett.* , *33*,
220 L01403.
- 221 Rossi, M., S. Peruccacci, A. Witt, B.D. Malamud and F. Guzzetti (2008), Character-
222 istics of an historical landslide catalogue for the Emilia-Romagna Region, Northern
223 Italy: frequency-size, temporal clustering and triggering factors, *Geophys. Res. Abs.*,
224 *10*, EGU2008-A-07210.
- 225 Woodward, R., D.E. Newman, R. Sánchez and B.A. Carreras (2004), Comment on “Do
226 earthquakes exhibit self-organized criticality?”, *Phys. Rev. Lett.*, *93*, 249801.
- 227 Yang, X., S. Du, and J. Ma (2004), Do earthquakes exhibit self-organized criticality?,
228 *Phys. Rev. Lett.*, *92*, 228501.

Table 1. Generic driving rate ν in terms of experimental parameters

Description	Driving rate (no units) ν	Pour rate (g s^{-1})	Vibration frequency (Hz)
Slow	7.50×10^{-5}	3.21	1.8
Moderate	1.25×10^{-4}	6.60	1.8, 10, 89
Fast	7.50×10^{-4}	21.09	1.8, 10, 89

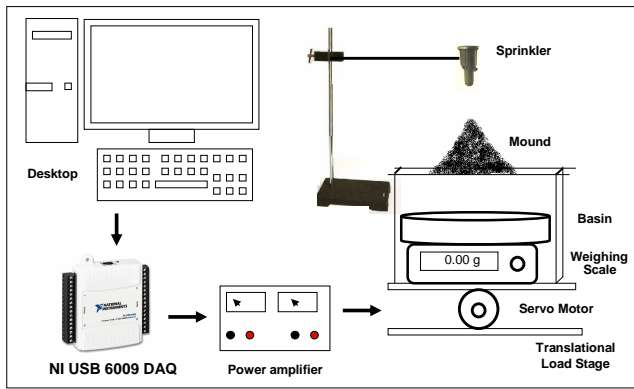


Figure 1. Diagram of experimental setup. Sand mound consists of river sand. Rainfall is simulated by a sprinkler right above the mound apex. An earthquake is simulated by a translational load stage imparting horizontal vibrations to the platform where the mound is placed. Rainfall and vibration are parametrized by pour rate and vibration frequency, respectively. Different parameter combinations are listed on Table 1. Avalanche size is the mass M of wet sand falling onto the basin within 20-ms intervals. M is measured by a weighing scale at the bottom of the basin, and is connected to the PC that records measurements in time.

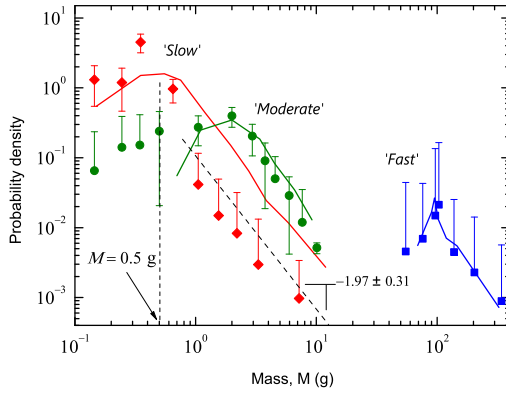


Figure 2. (Color online). Probability densities (pdf) of avalanche sizes. Pdfs for slow (\blacklozenge), moderate (\bullet), and fast (\blacksquare) driving; where the error bars are $\pm 2\sqrt{n}/\delta$ (equivalent to $\pm 2\sigma$, 95% confidence; n = number of values in a bin; and δ is the bin width). Corresponding pdfs of avalanche size from numerical simulations (curves) are overlaid, after converting area into mass using the scaling relation: $M = (1.0 \times 10^{-5} \text{g} \cdot \text{cell}^{-3/2})A^{3/2}$. Linear regime ($1.0 < M < 8.0$ g) of the pdf for a slowly-driven mound fits a power-law with exponent -1.97 ± 0.31 . For moderately-driven mounds, the rollover region of the pdf becomes more prominent as the peak shifts to the right. For highly-driven mounds, the pdf resembles a normal distribution centered at a large M .

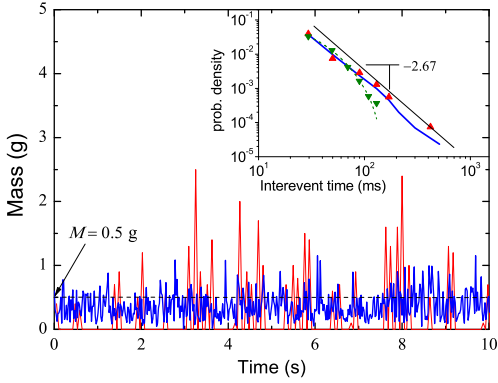


Figure 3. (Color online). Interevent occurrence times (IOT). Time series of avalanche sizes from experiment (red, solid curve) and model (blue, thick curve). Consecutive data points are separated by 20 ms. Iteration steps (iter) in the model have been rescaled to time by multiplying by the scaling factor: $0.05 \text{ s} \cdot \text{iter}^{-1}$. Avalanche sizes less than 0.5 g are discarded. IOT is the interval between consecutive peaks above the threshold. *Inset:* IOT distributions for experiment (\blacktriangle) and model (blue solid curve) both exhibit a power-law with exponent -2.670 ± 0.001 . Randomly shuffling the order of the time series effectively results in an exponential IOT distribution (\blacktriangledown ; curve fit: green, dashed curve).